Current Research in Food Science 5 (2022) 677–686

Contents lists available at ScienceDirect

Current Research in Food Science

journal homepage: www.sciencedirect.com/journal/current-research-in-food-science

Incorporation of gelatin and Fe^{2+} increases the pH-sensitivity of zein-anthocyanin complex films used for milk spoilage detection

Ruichang Gao [a,b,*], Huiling Hu [a], Tong Shi [a], Yulong Bao [a], Quancai Sun [a], Lin Wang [a], Yuhan Ren [a], Wengang Jin [b], Li Yuan [a,**]

[a] School of Food and Biological Engineering, Jiangsu University, Zhenjiang, Jiangsu Province, 212013, China
[b] Bio-resources Key Laboratory of Shaanxi Province, School of Biological Science and Engineering, Sha'anxi University of Technology, Hanzhong, Sha'anxi Province, 723001, China

ARTICLE INFO

Keywords:
Electrospun
Indicator film
Blueberry anthocyanins
Milk freshness
Gelatin
Intelligent packaging

ABSTRACT

In this study, blueberry anthocyanins, gelatin and Fe^{2+} were incorporated into zein matrix via electrospinning method to prepare colorimetric indicator films for monitoring milk freshness. Gelatin and Fe^{2+} were incorporated into the film to improve visual discrimination of indicator films' color changes in milk with different freshness degrees and in solution with pH 3–7. Results of SEM, FT-IR and XRD showed that there were intermolecular hydrogen bonds among components, which associated with the larger color difference of indicator films. UV–vis spectral analysis showed that blueberry anthocyanin solutions containing both gelatin and Fe^{2+} displayed the highest intensity absorption peaks. The optimal ability to distinguish the pH (3–7) of solutions was presented by the indicator film incorporating gelatin (1% (w/v)) and Fe^{2+} (0.07 mg/mL). Gelatin and Fe^{2+} increased the color-responsive sensitivity of the indicator film to pH. The film could be successfully used to detect the freshness of milk, whose color changes were visually perceivable: from purple black (fresh milk) to royal purple (spoiling milk) and then to violet red (spoiled milk). The color parameters (L^*, a^*, R, G and B) of the film revealed a high correlation with the pH/acidity of the milk during storage. The successful application of the indicator film embedding gelatin and Fe^{2+} for monitoring milk quality changes indicated that the addition of special substances could provide great potential for monitoring freshness and preparing intelligent packaging of food.

1. Introduction

There were estimates that one-third of food produced for human consumption, accounting for 1.3 billion tons per year, was wasted (Gustavsson et al., 2011). In terms of the share of the total value of food loss at the retail and consumer levels, dairy products accounted for 17% and were in one of the top three food categories for food waste in the United States in 2010 (Buzby et al., 2014). Thus, monitoring the freshness of milk might effectively reduce food waste to some extent. Currently, several methods exist for detecting milk freshness, such as near-infrared spectroscopy (Wang et al., 2015), mid-infrared and nuclear magnetic resonance (Loudiyi et al., 2020). However, these methods present tedious operations and expensive equipment is required. Therefore, it is a real necessity to develop faster and less costly methods for accurately monitoring the freshness of milk and other foods during processing and storage. As observed, intelligent packaging and freshness indicators are attracting attention because of the efficiency, economy and simplicity of the performance (Goodarzi et al., 2020; Pateiro et al., 2019). Jia et al. (2019) prepared cellulose-based ratiometric fluorescent materials with high amine responsiveness for real-time and visual detection of seafood freshness. Smart color-changing pH sensors based on azo-anthraquinone reactive dyes were produced to quickly identify the freshness and safety of food during transportation or before consumption (Zhang et al., 2019). However, these smart materials are not easily approved by consumers because of potential safety risks. Given its safety and nontoxicity, it is undoubtedly a good choice to prepare pH indicators containing natural pigments such as curcumin (H. Chen et al., 2020; Ezati and Rhim, 2020) and anthocyanins (Choi et al., 2017; Devarayan and Kim, 2015; Ma et al., 2017; Shi et al., 2020; Zeng et al., 2019) for monitoring the freshness of food in

* Corresponding author. School of Food and Biological Engineering, Jiangsu University, No.301, Xuefu Road, Zhenjiang, Jiangsu Province, 212013, China.
** Corresponding author.
E-mail addresses: xiyuan2008@ujs.edu.cn (R. Gao), 1000003464@ujs.edu.cn (L. Yuan).

https://doi.org/10.1016/j.crfs.2022.03.016
Received 30 December 2021; Received in revised form 10 March 2022; Accepted 25 March 2022
Available online 5 April 2022

the course of storage. The anthocyanins isolated from *Clitoria ternatea* could be used for monitoring beverage and seafood freshness due to its excellent response characteristics in a wide range of pH (including from neutral to (weakly) acidic conditions) (Singh et al., 2021; Wu et al., 2020). However, many anthocyanins, such as blueberry anthocyanins (Ma et al., 2020; Shi et al., 2020) and purple potato anthocyanins (S.L. Chen et al., 2020; Jiang et al., 2020; Zhang et al., 2019) do not vary significantly in color from neutral to (weakly) acidic conditions, which incapacitates the pH indicator film encapsulating these colorants for monitoring the freshness of acid-producing foods during spoilage. Acidic spoilage of pasteurized whole milk is a typical case of pH from neutral to acidic conditions: lactose is broken down by lactic acid bacteria to produce lactic acid, resulting in a decrease in pH (from 6.6 to 6.8 to 4.0–5.0) (Basdeki et al., 2021; Lu et al., 2013; Ma et al., 2020). To make it possible to monitor the microbial quality of milk and other acid-producing foods during spoilage and reduce food waste, it is of particular importance to improve the color difference of pH indicator films embedding these natural pigments from neutral to (weakly) acidic conditions.

It has been reported that iron ions and anthocyanins formed stable and colored chelates (El-Naggar et al., 2021; Xie et al., 2018). And deeper and more intense blue hues were observed from gelatin-based gels immobilizing ferric anthocyanin chelates than from gels based on blends of agar-agar with amidated pectin containing ferric anthocyanin chelates (Buchweitz et al., 2013a). Additionally, lactic acid had a negative effect on the blue colors mentioned above due to the annihilation role (Buchweitz et al., 2013b). Hypothetically, with the increase of lactic acid concentration during milk spoilage, the indicator film containing gelatin and iron/ferrous ion with anthocyanin as an indicator will show richer color changes than that embedding only anthocyanin, so that people can easily distinguish the freshness of milk according to the color of indicator film. At the same time, it also broadens the application of some colorants (such as blueberry and purple potato anthocyanins) that present colors that are not easily distinguishable from neutral to weakly acidic conditions. Electrospinning is considered a promising technology to fabricate high sensitivity sensors with the advantages of high porosity, surface-to-volume ratio and encapsulation rate of active components, facile fabrication and so on (Agarwal et al., 2013; Kumar et al., 2019; Ulrich et al., 2020). Zein, a nontoxic and biodegradable polymer (Shaikh et al., 2021), has film forming properties and can be used for the preparation of nanofibers and capsules by electrospinning (Aghaei et al., 2020; Alehosseini et al., 2019). In this study, color-responsive and high-sensitivity zein-based indicator films containing blueberry anthocyanin, gelatin and Fe^{2+} were prepared by electrospinning and successfully applied to the visual detection of milk freshness.

2. Materials and methods

2.1. Materials

Blueberry anthocyanins were purchased from Macklin Biochemical Co., Ltd. (Shanghai, China). Snakehead fishes (used to obtain gelatin) and pasteurized bovine milk (Bright Dairy) were purchased from local market (Zhenjiang, China). Zein was bought from Sigma Chemical Co. (St. Louis, MO, USA). $FeSO_4{\cdot}7H_2O$ (CAS number 7782-63-0), acetic acid (CAS number 64-19-7) and other analytical reagents were purchased from Sinopharm Chemical Reagent Co. Ltd. (Shanghai, China).

2.2. Extraction of snakehead fish skin gelatin

Snakehead fish skin was cut into pieces with a 2 × 2 cm^2 size for the extraction of gelatin. Gelatin extraction was performed according to the method of Tan et al. (2019) with some modifications. Briefly, the prepared fish skin was soaked in 0.05 M NaOH at a skin-to-solution ratio of 1:5 (w/v) for 8 h before washing to neutral with tap water. Then, the fish skin was incubated at 55 °C for 6 h in distilled water at skin-to-water ratio of 1:4 (w/v). Next, the obtained gelatin was filtered with gauze and filter paper. And the filtrate was freeze-dried for further use.

2.3. Preparation of indicator films

2.3.1. Preparation of electrospinning solution

The spinning solution was prepared by dissolving zein (30% w/v), anthocyanin (5% w/v), gelatin (1% w/v) and $FeSO_4{\cdot}7H_2O$ (0.07 mg/mL) in 70% (v/v) acetic acid solution. And the mixture was stirred at 500 rpm at room temperature for 4 h to dissolve completely. The selected concentration of zein and anthocyanin, gelatin and $FeSO_4{\cdot}7H_2O$ was based on our previous experiments (Supplementary contents).

2.3.2. Electrospinning

All the solutions were separately loaded into two 2 mL syringes connected to a 20-gauge blunt tip stainless steel needle. Nanofiber films were fabricated by a high voltage electrostatic spinning machine for 8 h with the following predetermined parameters: applied voltage 18 ± 0.5 kV, feed rate 0.25 mL/h, tip to collector distance 15 cm. The electrospinning process was conducted at 25 ± 5 °C and 35 ± 5% RH. Then, the nanofibers collected on the aluminum foil were stored in a desiccator away from light for further use. And the nanofiber film was removed from the foil as an indicator film. It is worth mentioning that the four films obtained from four spinning solutions (zein + anthocyanin; zein + anthocyanin + gelatin; zein + anthocyanin + $FeSO_4{\cdot}7H_2O$; zein + anthocyanin + gelatin + $FeSO_4{\cdot}7H_2O$) were referred to as F1, F2, F3, and F4, respectively. The film without gelatin or $FeSO_4{\cdot}7H_2O$ was prepared as the control, that is F1.

2.4. Characterization of films

2.4.1. Scanning electron microscopy (SEM)

The surface morphology of the nanofiber films (indicator films) was determined by the field emission scanning electron microscopy (Regulus-8100, Japan). All samples were glued to conductive adhesive to sputter-coated a thin layer of gold before being fixed on to SEM stubs. Then, the representative SEM images were taken at magnification of × 10.0 k.

2.4.2. Fourier transform infrared (FT-IR) spectroscopy

FT-IR spectra of dried electrospinning nanofiber films, zein powders and freeze-dried gelatin were obtained from a FT-IR spectrometer (Nicolet iS50, USA) to analyze the interaction among components. Each sample was scanned 32 times at a resolution of 4 cm^{-1} in the wavenumber range of 4000–400 cm^{-1}.

2.4.3. X-ray diffraction (XRD)

The crystal phase of samples was investigated by X-ray diffractometer (Bruker D8 Advance, Germany) in the range of 5–90° (2θ) with a scanning rate of 5°/min.

2.5. Color response to solution at different pH values

According to Weston et al. (2020) with some modifications, The colorimetric analyses of the indicator films in solutions with different pH values were conducted by immersing the film pieces (0.5 × 0.5 cm^2) in a 5 mL solution adjusted to a pH range of 3–7 by adding lactic acid (10%) and NaOH (0.5 mol/L) dropwise. After a 3 min incubation, the color of the films was photographed and subjected to digital colorimetric analysis with Photoshop 2019 software (Adobe Systems Incorporated, America). Furthermore, the total color difference (ΔE) was calculated as follows:

$$\Delta E = \left[\left(L_t^* - L_0^*\right)^2 + \left(a_t^* - a_0^*\right)^2 + \left(b_t^* - b_0^*\right)^2\right]^{\frac{1}{2}} \quad (1)$$

where L_t*, a_t*, and b_t* are the color values of the indicator films at pH = t, and L_0*, a_0*, and b_0* are the color values of the indicator films at pH = 3 ($3 \leq t \leq 7$).

2.6. Application of the indicator films to milk freshness monitoring

2.6.1. Detection of pH and acidity of milk

Pasteurized fresh milk was poured into several 50 mL sterilized centrifugal tubes and placed in an incubator of 25 °C until the milk got spoiled. At different time points (0, 24, 48, 64, 80, 88 h), three sterilized centrifugal tubes containing milk were randomly taken out for the determination of pH and acidity of milk. The pH value of the milk was measured using a digital pH meter. And the acidity (°T) was determined using acid-base titration method as described by Ma et al. (2020) with some modifications. The milk sample (10 g) at different time points was placed into a 150 mL conical flask, followed by adding 20 mL distilled water with carbon dioxide removed. The titration was carried out with 0.1 mol/L NaOH using alcoholic phenolphthalein (0.5% w/v) as the indicator. All tests were carried out in triplicate.

2.6.2. Application of indicator films for monitoring the freshness of milk

The indicator films (0.5 × 0.5 cm^2) were soaked in 5 mL milk and removed periodically (0, 24, 48, 64, 80, 88 h) from the incubator for 3 min to conduct application tests on milk. The films were photographed, and the color images were processed by Photoshop 2019. Then, the ΔE was calculated as mentioned in Section 2.5. (where L_t*, a_t*, b_t* are the color values of the indicator films immersed in milk with a storage time of t h, and L_0*, a_0*, b_0* are the color values of the indicator films immersed in milk with a storage time of 0 h). Finally, the correlation between the color parameters of the indicator films and the pH/acidity of the milk was analyzed.

2.7. Statistical analysis

Experiments were performed in triplicate, and the results were reported as mean ± SD based on multiple samples (n = 3). The data were subjected to analysis of variance (ANOVA) with Duncan's multiple range test ($P < 0.05$) of the IBM SPSS Statistics 22.0 to determine the significant differences of mean. The correlation analysis was performed with GGally package of Rstudio software and other charts were drawn by the Origin 2018 and ChemDraw 2016.

3. Results and discussion

3.1. Characterization of indicator films

3.1.1. SEM analysis

The morphology of the electrospun nanofiber films (indicator films) is shown by the SEM images in Fig. 1A–D. The nanofiber films showed an obvious beaded structure especially the nanofiber films embedding gelatin (Fig. 1B and D). It might be that the addition of gelatin promoted the interaction among the components. And there might be cross-linking in situ or even deposition in situ between film-forming substrates, resulting in the generation of nanoparticles in the electrospun nanofibers (Lee et al., 2016; Renata et al., 2016; Yang et al., 2020). In addition, the degree of volatilization of solvent had a certain effect on the beads and their morphology in nanofibers (Angel et al., 2020; Kumar et al., 2019). However, the addition of Fe^{2+} had little effect on the morphology and diameter of nanofibers (Fig. 1C). As seen from the diameter distribution diagram (Fig. 1a-d), the average diameter (approximately 60–80 nm) of the nanofibers obtained in this study was smaller than those reported by Prietto et al. (2017) who studied pure zein ultrafine fibers and zein nanofibers with 5% anthocyanins, with diameters ranging from 444 to 510 nm. It was described that a smaller nanofiber diameter contributed to a higher pH sensitivity due to the increased specific surface area of the film (Sun et al., 2020). However, the diameter of the nanofibers increased slightly after gelatin (1%) was added (Fig. 1b and d), which was consistent with the result described by Deng et al. (2018) who found that the nanofiber diameters gradually increased from 380.3 nm to 695.5 nm as the weight ratio of gelatin increased from 33.3% to 100%. This might be due to the increased viscosity of the spinning solution and assembled structure (Deng et al.,

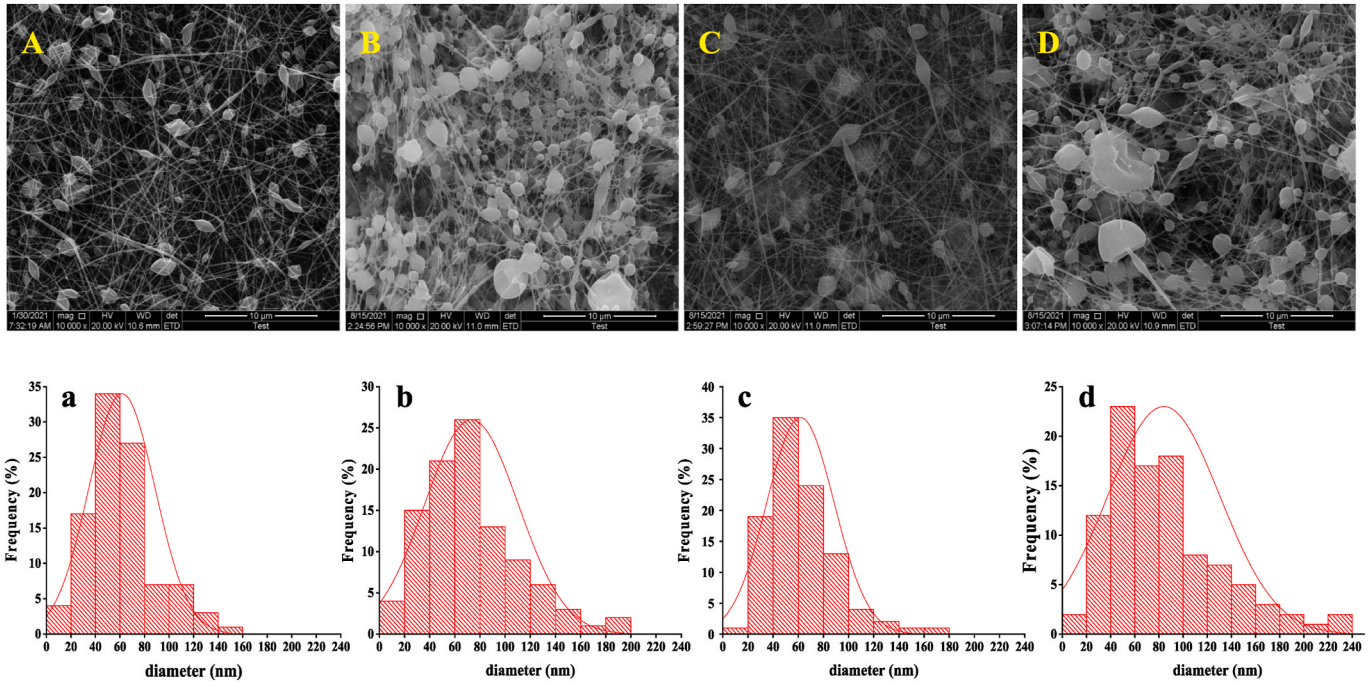

Fig. 1. SEM images (A–D) and corresponding diameter distribution diagram (a–d) of electrospun films (F1, F2, F3 and F4). F1, F2, F3 and F4 were electrospun films from four spinning solutions mixing zein + anthocyanin, zein + anthocyanin + gelatin, zein + anthocyanin + $FeSO_4 \cdot 7H_2O$, and zein + anthocyanin + gelatin + $FeSO_4 \cdot 7H_2O$, respectively.

2018). It was generally considered that the viscosity of the solution was one of the dominant parameters determining the morphology of nanofibers (Amariei et al., 2017). Apart from viscosity, other parameters that affect the morphology of nanofibers include solution parameters (conductivity, surface tension and so on), process parameters (voltage, feed rate and tip to collector distance), and environmental parameters (temperature and humidity) (Kumar et al., 2019).

3.1.2. FT-IR spectroscopy characterization

The FT-IR spectra of samples (blueberry anthocyanins and zein powders, freeze-dried gelatin, F1, F2, F3 and F4) are shown in Fig. 2A, where a broad peak at 3200-3600 cm^{-1} emerged for all samples, associated with the stretching vibration of –OH and –NH groups. Zein and gelatin exhibited characteristic peaks at 1661.9 cm^{-1} and 1530.2 cm^{-1}, corresponding to the axial stretching of the C═O bond in the amide I band and the symmetric angular deformation of the link N–H and stretching vibration of C–N in the amide II absorption band, respectively (Ma et al., 2020; Prietto et al., 2017). The spectrum of anthocyanin powders presented characteristic absorption peaks at 1623.8 cm^{-1} and 1029.3 cm^{-1} corresponding to the C═C stretching and C–H deformation vibrations of the aromatic species, respectively (Agarwal et al., 2012). For the electrospun indicator films (F1, F2, F3 and F4), the characteristic peak of amide I still existed but displayed a bathochromic shift to 1656.6 cm^{-1} compared with zein/gelatin, which might be related to hydrogen bonding and other interactions between zein/gelatin and anthocyanins (Zeng et al., 2019). Simultaneously, the spectra of F1, F2, F3 and F4 all introduced a new stronger absorption peak of anthocyanins at approximately 1029.3 cm^{-1} compared with the spectra of zein/gelatin. These phenomena certified that anthocyanins were incorporated into the nanofiber matrix and might interact with other substances (zein, gelatin and Fe^{2+}) to some certain extent. In addition, the characteristic peaks of zein/gelatin at 3308.8/3310.2 cm^{-1} shifted to 3303.4 cm^{-1} confirming that new intermolecular hydrogen bonds may be formed between the film-formed substrates so that the intermolecular interaction was enhanced (Bao et al., 2021).

3.1.3. X-ray diffraction (XRD) analysis

Fig. 2B shows the XRD patterns of the samples. Specifically, the XRD pattern of the blueberry anthocyanins presented a broad peak at ~18°, indicating that the anthocyanins were in an amorphous state (Ma et al., 2020). Zein and gelatin diffraction patterns showed a diffuse halo at approximately 2θ = 20°, associated with an amorphous phase (Sanuja et al., 2015). The diffraction peak of gelatin at approximately 2θ = 8.5° was related to the ordered triple-helical crystalline structure of the protein (Bigi et al., 2004). As we could see from the patterns of F1, F2, F3 and F4, the broad diffraction peak at approximately 2θ = 20°, corresponding to the amorphous state, still existed, yet the intensity of the diffraction peak of the indicator films decreased except F2. This result indicated that new hydrogen bonds between anthocyanins and film-formed components were formed to decrease crystallinity (Ge et al., 2020), which was consistent with the FT-IR analysis results.

3.2. Color response of nanofiber films in solutions with different pH values

Color parameters (L^*, a^*, b^*, R, G, B) evaluated by immersing the indicator films (F1, F2, F3 and F4) in solutions (pH 3–7) are listed in Supplementary Table SF1. L^*, a^*, and b^* indicate the lightness of the sample ranging from 0 (black) to 100 (white), chroma of greenness (negative a^*)/redness (positive a^*) and chroma of blueness (negative b^*)/yellowness (positive b^*) of the films, respectively (Prietto et al., 2017). The change in the L^*, a^*, b^*, R, G and B values could reflect the change in indicator film colors. As shown in Fig. 3A, the colors of F1 and F2 were difficult to distinguish in five solutions with different pH values (3–7) while color discrimination could be easily observed from two other indicator films, especially F4. The color change of F3 was pink (pH = 3), red violet/grape (pH = 4), red sandalwood hue (pH = 5), and purple black (pH = 6 and 7). The color of F4 varied from pink (pH = 3) → red violet/grape (pH = 4) → red sandalwood hue (pH = 5) → purple black (pH = 6) → blue black (pH = 7). The color changes were visually perceivable when the ΔE value was more than 5 (Moradi et al., 2019). From Fig. 3B, the greater ΔE values in F3 and F4 were consistent with the more visual color changes with the naked eye mentioned above. The greatest ΔE value indicated that it was easier to distinguish between different pH values by F4 (Fig. 3B), which was considered to be superior for freshness monitoring of milk.

3.3. Changes in pH and acidity during milk storage

It was reported that changes in pH and acidity were the most reliable symbols during milk spoilage (Goodarzi et al., 2020). Thus, pH and acidity were devoted to evaluating the freshness of milk in this study. The change tendencies of them with storage time of milk are shown in Fig. 4. The initial pH/acidity of pasteurized milk was 6.62/13.37. Then, the pH value of milk continuously decreased while the acidity continued to increase with a longer storage time, which was due to the accumulation of lactic acid from microbial metabolism (Ma et al., 2020). Generally, milk was considered fresh when its acidity ranged from 12°T

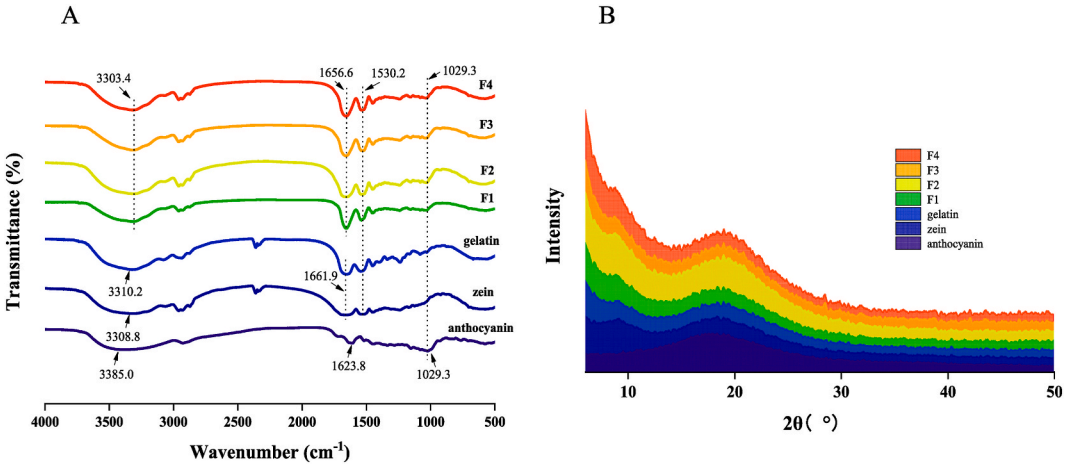

Fig. 2. FT-IR spectra (A); and XRD patterns (B) of blueberry anthocyanin and zein powders, freeze-dried gelatin and electrospun films (F1, F2, F3 and F4) F1, F2, F3 and F4 were electrospun films from four spinning solutions mixing zein + anthocyanin, zein + anthocyanin + gelatin, zein + anthocyanin + $FeSO_4 \cdot 7H_2O$, and zein + anthocyanin + gelatin + $FeSO_4 \cdot 7H_2O$, respectively.

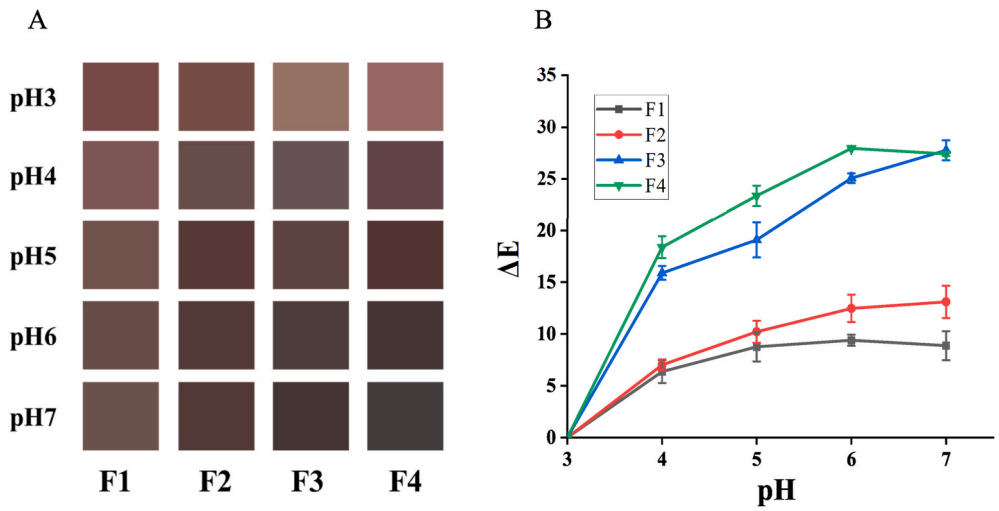

Fig. 3. The changes in colors (A) and ΔE (B) of indicator films (F1, F2, F3 and F4) in solution with different pH values (pH = 3, 4, 5, 6, 7). F1, F2, F3 and F4 were electrospun films from four spinning solutions mixing zein + anthocyanin, zein + anthocyanin + gelatin, zein + anthocyanin + $FeSO_4{\cdot}7H_2O$, and zein + anthocyanin + gelatin + $FeSO_4{\cdot}7H_2O$, respectively. (For interpretation of the references to color in this figure legend, the reader is referred to the Web version of this article.)

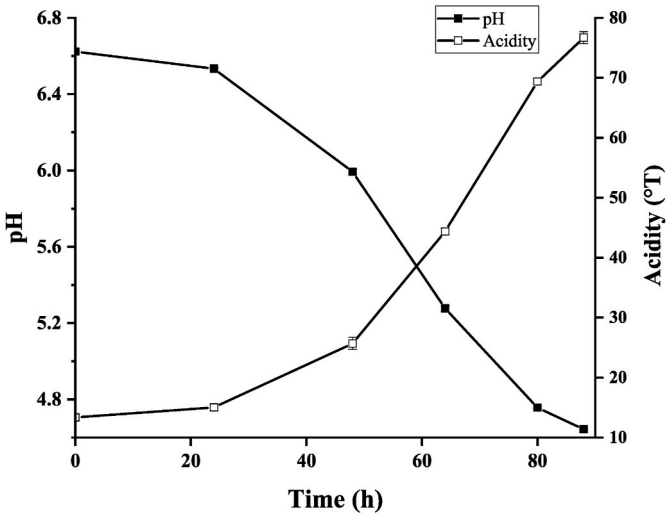

Fig. 4. The curves of pH and acidity during milk storage (25 °C).

to 18°T. Combined with the pH obtained from the experiment at different storage times, milk obtained at 0 h (pH 6.62) and 24 h (pH 6.53) was fresh. As Lu et al. (2013) described, lactic acid bacteria, at lower pH levels of 4.0–5.0, induced undesirable spoilage in milk. Therefore, milk with a pH of 4.0–5.0 was defined as spoiled milk and with a pH of 5.0–6.0 was considered spoiling milk in this study. That is, milk was fresh when stored for 0–24 h, medium-fresh when stored for 48–64 h, and spoiled after an 80 h store.

3.4. Color response

3.4.1. Color response of nanofiber films in milk

To verify the suitability of monitoring milk freshness with nanofiber films containing Fe^{2+} and gelatin, the films (F1, F2, F3, F4) were soaked in milk after storage for different time (0, 24, 48, 64, 80, 88 h). The color changes and detailed color parameters of F1, F2, F3 and F4 are shown in Fig. 5A and Table SF2 respectively. Overall, the L^*, a^*, R, G and B values of F1, F2, F3 and F4 showed an increasing trend. The b^* values of F4 were smaller than those of the other indicator films. In other words, the color of F4 was bluer than that of other indicators to some extent. This was dovetailed nicely with what Buchweitz et al. (2013a) expounded that an intense blue hue was observed in the gelatin gels containing ferric anthocyanin chelates. From the color strips in Fig. 5A, F3 and F4 exhibited a distinct color change upon increasing the concentration of lactic acid during milk storage while F1 and F2 did not. The color of F1 was violet red after being soaked in the milk obtained in different time intervals while F2 showed a slight color difference (from deep violet red to violet red) in milk with storage times of 0 and 24 h. Therefore, the indicator film F1 and F2 were poor at monitoring the freshness of milk. For F3 and F4, the ΔE values were basically greater than those of F1 and F2 (Fig. 5B) indicating an easier discernible color change. The visible color was in the order of purple black, blue violet, and pale violet red/violet red after being soaked in milk that was stored for different times. According to the description of milk freshness above (0–24 h: fresh milk; 48–64 h: spoiling milk; 80–88 h: spoiled milk), it would be great if the color changes in three stages could be distinguished with the naked eye. Excitedly, the performances of F3 and F4 met our expectations. F3 exhibited purple black at 0 h and 24 h (fresh milk), turned into a violet red hue at 48 h and 64 h (spoiling milk) and finally presented a pale violet red at 80 h and 88 h (spoiled milk). The color of F4 went from purple black (fresh milk) to royal purple (spoiling milk) and then to violet red (spoiled milk). This result indicated that we could visually discriminate freshness degrees of milk from the colors of the indicators (F3 and F4). Similar results were reported in the intelligent film of κ-carrageenan incorporated with Lycium ruthenicum Murr. extract (Liu et al., 2019). In addition, the ΔE values of F4 were greater than those of F3 (Fig. 5B). This favorable phenomenon for freshness monitoring of milk was consistent with Buchweitz et al.'s suggestion that proteins were more suitable for coloring with anthocyanin chelates (Buchweitz et al., 2013a). In addition, milk is rich in protein that can interact with anthocyanin (He et al., 2016). And it was reported that some substances, such as proteins, had an impact on the excited states of chromophores, which could change the properties of UV–Vis absorption spectra to higher or lower wavelengths and ultimately led to the change of color of indicator films (Madeira et al., 2019). Moreover, milk contains some metal ions, such as Ca^{2+} and Zn^{2+}, might contribute to the bathochromic shift of the maximum absorption wavelength in the visible spectrum and the increase of absorbance, due to decrease of the electron transition energy in anthocyanins π-conjugated system upon metal coordination (El-Naggar et al., 2021; Torrini et al., 2022). Therefore, these conditions (the composition and content of the monitored sample, such as type and content of protein and metal ions) might affect the color of the nanofiber films to some certain extent, so that the color changes of the nanofiber films in milk were easier to distinguish than that of in solution with

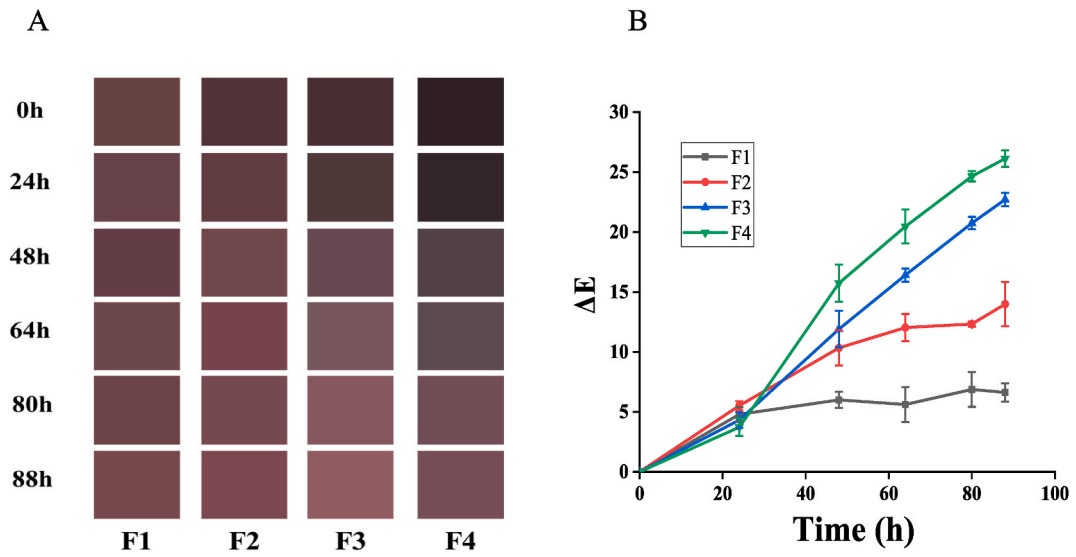

Fig. 5. The changes in colors (A) and ΔE (B) of indicator films (F1, F2, F3 and F4) immersed in milk after storage for different times (0 h, 24 h, 48 h, 64 h, 80 h, 88 h). F1, F2, F3 and F4 were electrospun films from four spinning solutions mixing zein + anthocyanin, zein + anthocyanin + gelatin, zein + anthocyanin + $FeSO_4{\cdot}7H_2O$, and zein + anthocyanin + gelatin + $FeSO_4{\cdot}7H_2O$, respectively. (For interpretation of the references to color in this figure legend, the reader is referred to the Web version of this article.)

different pH (3–7) mentioned above.

3.4.2. *Effects of Fe^{2+} and gelatin on the color response of anthocyanin solution*

Some properties of the solution were studied to reasonably explain the color change of the indicator labels. The color variation of blueberry anthocyanin solutions at pH 3–11 is illustrated in Fig. 6A. A distinct color change from vermilion to dark purple was present in the solutions with a pH of 3–11. The color of the solution changed from vermilion to pink as the pH increased from 3 to 4. The pink color of the solution gradually became light with increasing pH from 4 to 8, while the color was too similar to monitor the freshness of milk. After that, the color of the solution gradually changed from light purple to dark purple at pH 9–11. The corresponding UV–vis spectra of blueberry anthocyanin solutions with a pH range of 3–11 are shown in Fig. 6B. With an increasing pH of the solutions, the absorption peak shifted toward a higher wavelength. A maximum absorption appeared at 512 nm at pH 3 but displayed a bathochromic shift to approximately 585 nm at pH 11. Additionally, the intensity of the absorption peak gradually decreased with pH 3–8, which was consistent with the lighter pink color mentioned above. An increase in the intensity of the absorption peak was observed in the solution with a pH of 9–11. In fact, the change in the absorption peak was closely related to the chemical structure of anthocyanins (Liu et al., 2019), which was referred to as the 'bathochromic shift' (Bakowska et al., 2003). The reaction equilibrium of anthocyanins can be analyzed and demonstrated by the Handerson-Hassel Balch equation

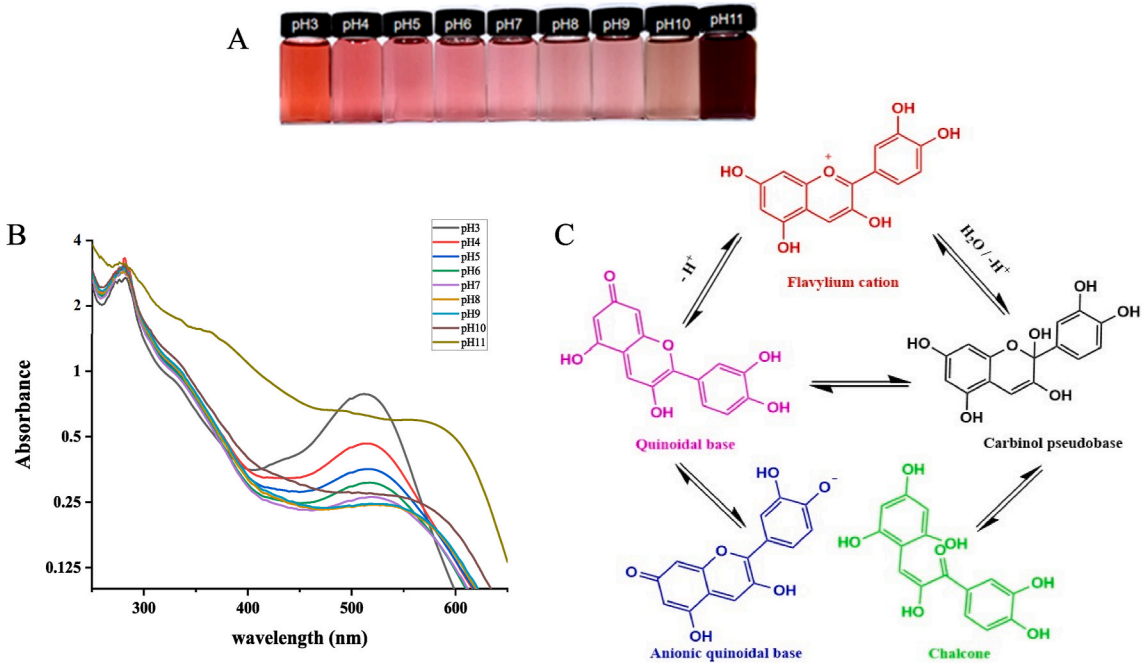

Fig. 6. Color changes (A) and UV–vis spectra (B) of anthocyanin solutions at different pH values; structural transformation of anthocyanin in solution with different pH values (C). (For interpretation of the references to color in this figure legend, the reader is referred to the Web version of this article.)

(Montagna et al., 2014) (Fig. 6C). Anthocyanins form various substances in solution, including flavylium cations (red), carbinol pseudobase (colorless), chalone (colorless), quinoidal base (purple), anionic quinoidal base (blue) and so on (Liu et al., 2019; Priyadarshi et al., 2021). These substances form a state of dynamic equilibrium. In acidic environments, anthocyanins exist as stable flavylium cations to generate a red color (Li et al., 2021). However, the double bonds of flavylium cations were susceptible to extended conjugation in the surrounding environment, forming the colorless carbinol pseudobase and chalone and resulting in the lighter pink mentioned above at pH 4–8 (Clifford, 2000). With a further pH increase, the solutions exhibit a purple/blue hue due to the quinoidal base/anionic quinoidal base formed from the further deprotonation of the flavylium cation (Mohd et al., 2011; Priyadarshi et al., 2021). The absence of blue color in the anthocyanin solution in this study may be due to the insufficient alkalinity of the solution or a special type of anthocyanin selected.

As mentioned earlier, the blueberry anthocyanins in this study, like those in other studies, did not show significant color changes at pH 3–7 and were not suitable for the monitoring freshness of milk. However, the blueberry anthocyanin indicator film embedding Fe^{2+} and gelatin can be successfully used to monitor the freshness of milk. Therefore, some relevant characteristics of anthocyanin solutions containing Fe^{2+} and gelatin were illustrated in this study. The blueberry anthocyanin solution, blueberry anthocyanin solution containing gelatin, blueberry anthocyanin solution containing Fe^{2+}, and blueberry anthocyanin solution containing gelatin and Fe^{2+} were abbreviated as S1, S2, S3 and S4, respectively. The colors of S1, S2, S3 and S4 with a pH range of 3–7 are shown in Supplementary Fig. SF5. An intense blue hue was observed in the solution containing gelatin and Fe^{2+}, which might benefit the increase of total color difference of indicator films. In addition, as demonstrated in Fig. 7 and Fig. SF6, the UV–vis absorption spectra showed that the intensity of the absorption peak of S4 was the highest, followed by that of S3, and the weakest intensity was from S1 at any pH of 3–7. Obviously, the absorption intensity of S1 gradually decreased while the intensity of S2, S3 and S4 progressively increased with increasing pH from 3 to 6. The absorption intensity of the solution at pH 6 and pH 7 was extremely close proximity. In addition, a significant bathochromic shift was observed in S3 and S4 at pH 4–7, and a greater bathochromic shift degree was found in S4. The results suggested that the addition of gelatin and Fe^{2+} could not only effectively increase the intensity of the absorption peak but also create a dramatic bathochromic shift. It was reported that ferric (ferrous) ions and anthocyanins could form colored chelates that partly explained these phenomena (Buchweitz et al., 2013a). At low total contents of ferric (ferrous) ions, fractional coordination of the ferric ions occurred to the phenolic hydroxyl substituents on the anthocyanins leading to partial pink chromogenic reaction (El-Naggar et al., 2021). When the amount of ferric (ferrous) ions increased to a certain extent, the amount of ferric (ferrous) anthocyanin chelates increased, further turning the color of the solution to purple or even blue (Khaodee et al., 2014). Then, gelatin contains chromophore and auxochrome groups, which might increase the absorption intensity of the solution and facilitate bathochromic shifts. Finally, driven by hydrophobic interactions, polyphenol (tannic acid) entered into the hydrophobic pocket formed by the side chains of hydrophobic amino acids on protein, and the phenolic hydroxyl groups of polyphenols bound with polar groups on protein chains through hydrogen bonds, which might lead to the partial unfolding of protein (Yi et al., 2010; Zhang et al., 2021; Zhao et al., 2013). Therefore, we inferred that anthocyanins and Fe^{2+}-anthocyanin chelates might enter into the hydrophobic pocket formed by the side chains of hydrophobic amino acids on gelatin. At this point, due to the aforementioned hydrophobic interactions and hydrogen bonds, the gelatin molecules might partially unfold leading to the exposure of the chromophore and auxochrome groups, and ultimately increased the absorption intensity and facilitate bathochromic shift (Xue and Dong, 2014; Zhang et al., 2021). On this basis, the interaction among these components will be an important part

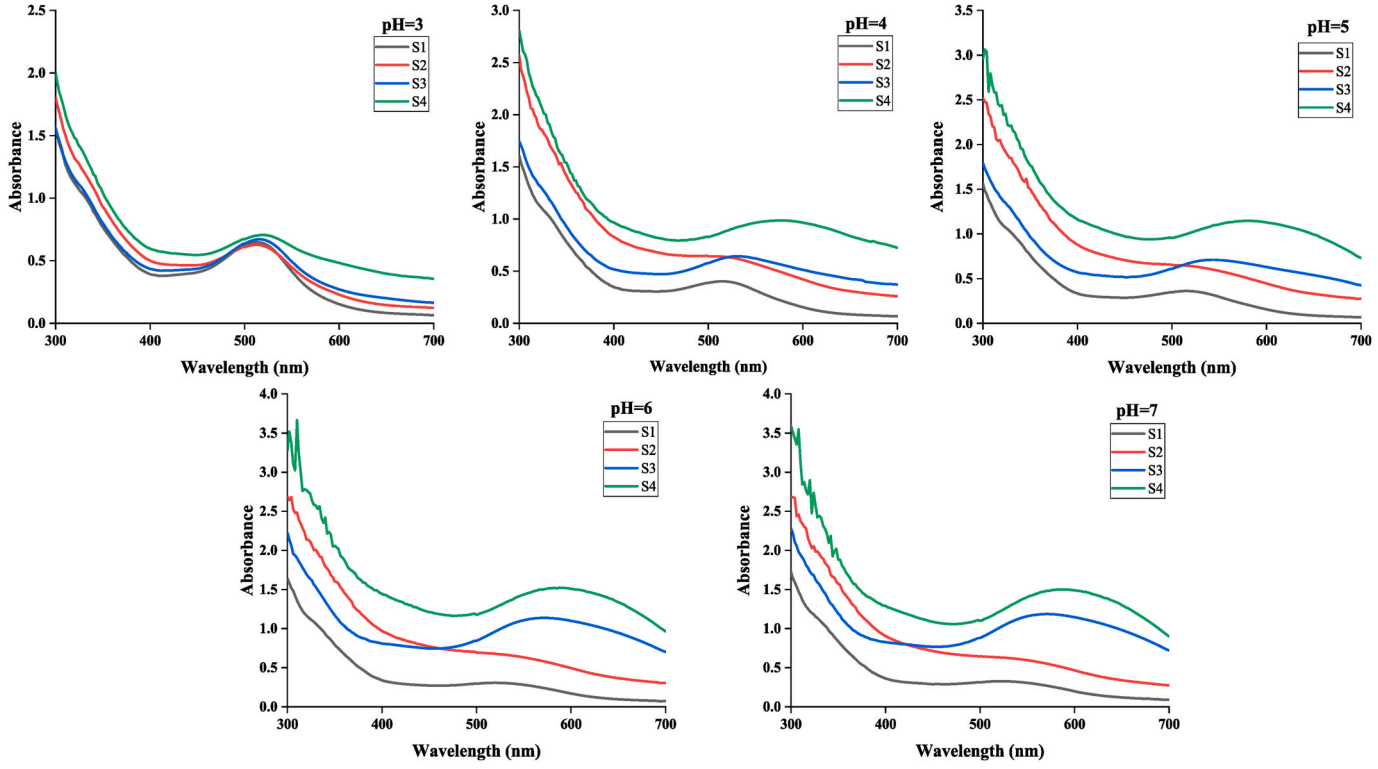

Fig. 7. The UV–vis spectra of S1, S2, S3 and S4 at pH 3 (A); pH 4 (B); pH 5 (C); pH 6 (D); and pH 7 (E). S1, S2, S3 and S4 refer to the blueberry anthocyanin solution, blueberry anthocyanin solution containing gelatin, blueberry anthocyanin solution containing Fe^{2+}, and blueberry anthocyanin solution containing gelatin and Fe^{2+}, respectively.

of our further research.

3.5. Correlation analyses between color parameters of films and freshness indices of milk

To further demonstrate that F3 and F4 were suitable for monitoring the freshness of milk, pairwise correlation analysis was conducted on the storage time, pH and acidity of milk and the corresponding color parameters (L^*, a^*, b^*, R, G, B) of F1, F2, F3 and F4 (Fig. 8). There was a strong pairwise linear correlation among the storage time, pH and acidity ($R^2_{Time\&acidity} = 0.936$; $R^2_{Time\&pH} = -0.968$; $R^2_{Acidity\&pH} = -0.984$). However, a poor correlation between the color parameters (L^*, a^*, b^*, R, G, B) of F1 and storage time/pH/acidity of milk was represented by the scatter plot distributed randomly (Fig. 8A). When gelatin was added, the correlation between some of the color parameters (such as L^*, a^*, R, G, B) of the indicator films and storage time/pH/acidity of milk evidently increased (Fig. 8B). As for the F3 and F4, color parameters except b exhibited a strong linear response to the storage time/pH/acidity of milk (Fig. 8B and C). Impliedly, consumers or retailers could not only judge the freshness of milk with the naked eye, but could also assess an accurate pH/acidity level of the milk based on color response, especially R, G and B values, extracted from indicator film images. As expected, the linear correlation coefficients illustrated that the correlation between the color parameters except b^* of F4 and the storage time/

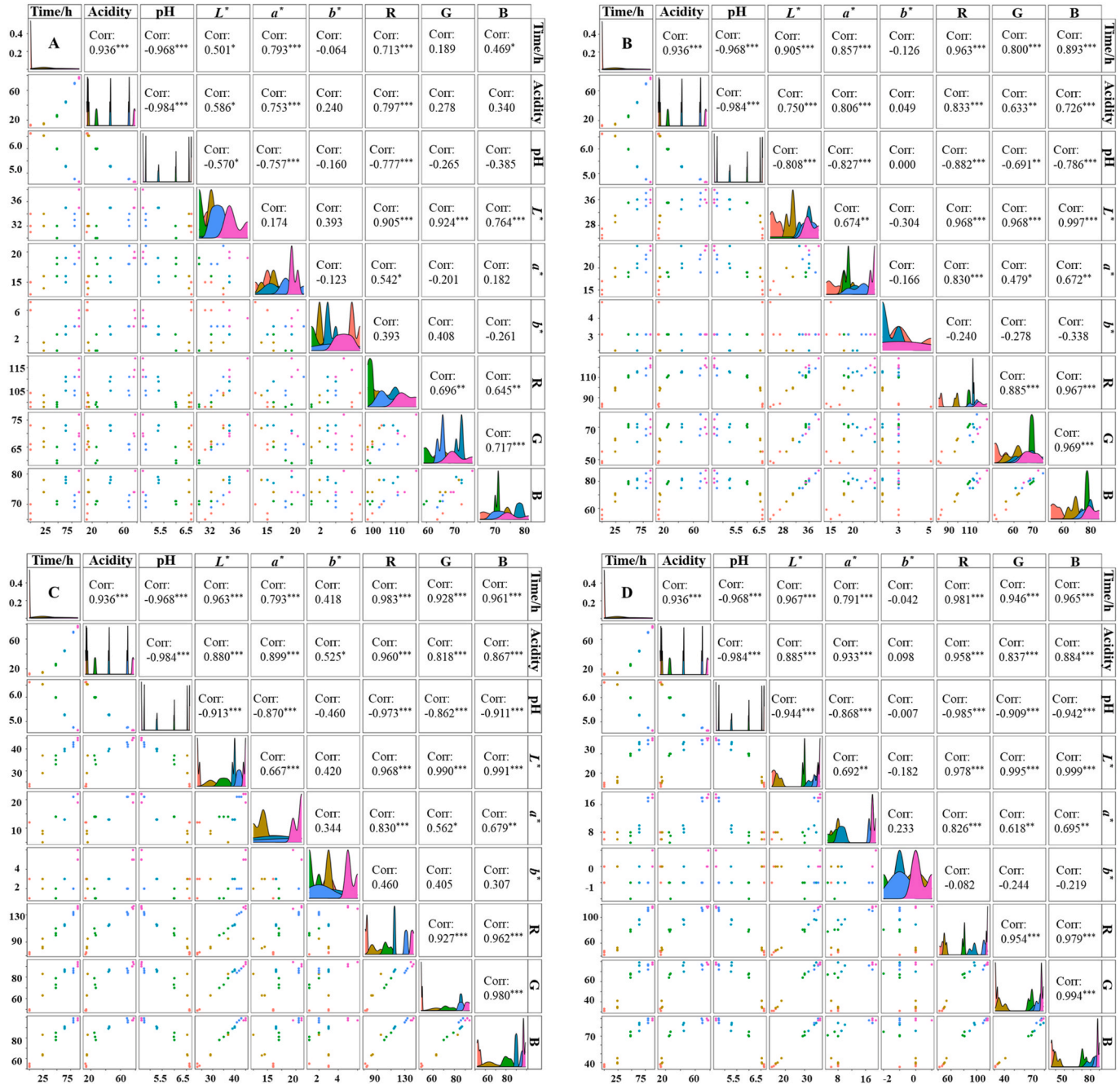

Fig. 8. Pairwise correlation analysis among storage time, pH, acidity of milk and corresponding color responses (L^*, a^*, b^*, R, G, B) of F1 (A), F2 (B), F3 (C) and F4 (D). F1, F2, F3 and F4 were electrospun films from four spinning solutions mixing zein + anthocyanin, zein + anthocyanin + gelatin, zein + anthocyanin + $FeSO_4{\cdot}7H_2O$, and zein + anthocyanin + gelatin + $FeSO_4{\cdot}7H_2O$, respectively. (For interpretation of the references to color in this figure legend, the reader is referred to the Web version of this article.)

pH/acidity of milk was generally stronger than that of F3. It might be that there were interactions between gelatin and anthocyanin/ferric anthocyanin chelates, which promoted bathochromic shift and increased intensity of absorption peak as mentioned above, and ultimately affected the color response of indicator film (Etxabide et al., 2021; Yang et al., 2018).

4. Conclusion

In this work, the high-sensitivity indicators embedding gelatin and Fe^{2+} with blueberry anthocyanin as an indicator were fabricated by electrospinning to monitor the freshness of pasteurized bovine milk. When the indicator films were exposed to solutions with different pH values (3–7) and milk after storage for different times, the color changes of indicator films incorporating gelatin and Fe^{2+} were more visually perceivable than those of the control indicator film, which was suggested by the larger ΔE values. In addition, the color parameters (L^*, a^*, R, G, B) of indicator films, especially the indicator film containing both gelatin and Fe^{2+}, revealed a high correlation with the pH/acidity of the milk during storage. All results showed that the interaction among gelatin and Fe^{2+} and anthocyanin affected the colors of the indicator film and made it easier to distinguish the solutions or samples with different pH values (3–7). Furthermore, the complex indicator films containing gelatin and Fe^{2+} had a superior ability to distinguish fresh, spoiling and spoiled milk, which could help to reduce food waste to some extent. This work provided a new perspective to the development of intelligent food packaging and freshness indicators used for various foods by combining some special substances with pigments.

CRediT authorship contribution statement

Ruichang Gao: Conceptualization, Interpretation, Validation, Writing – review & editing, Reviewing, Supervision. **Huiling Hu:** Conceptualization, Experimentation, Data treatment, Interpretation, Writing – original draft. **Tong Shi:** Methodology, Investigation. **Yulong Bao:** Conceptualization, Supervision, Writing – review & editing, Writing – original draft, Reviewing Draft. **Quancai Sun:** Interpretation, Validation. **Lin Wang:** Writing – review & editing, Writing – original draft, Reviewing Draft, Supervision. **Yuhan Ren:** Data treatment, Validation. **Wengang Jin:** Interpretation, Supervision, Validation. **Li Yuan:** Interpretation, Supervision.

Declaration of competing interest

The authors declare that they have no known competing financial interests or personal relationships that could have appeared to influence the work reported in this paper.

Acknowledgement

This work was supported by the China Agriculture Research System of MOF and MARA (Fund name: Comprehensive utilization of processing by-products of characteristic freshwater fish; Fund number: CARS-46), China; and the Senior Talent Program of Jiangsu University (20JDG062).

Appendix A. Supplementary data

Supplementary data to this article can be found online at https://doi.org/10.1016/j.crfs.2022.03.016.

References

Agarwal, A., Raheja, A., Natarajan, T.S., Chandra, T.S., 2012. Development of universal pH sensing electrospun nanofibers. Sens. Actuators, B 161, 1097–1101. https://doi.org/10.1016/j.snb.2011.12.027.

Agarwal, S., Greiner, A., Wendorff, J.H., 2013. Functional materials by electrospinning of polymers. Prog. Polym. Sci. 38, 963–991. https://doi.org/10.1016/j.progpolymsci.2013.02.001.

Aghaei, Z., Ghorani, B., Emadzadeh, B., Kadkhodaee, R., Tucker, N., 2020. Protein-based halochromic electrospun nanosensor for monitoring trout fish freshness. Food Control 111, 107065. https://doi.org/10.1016/j.foodcont.2019.107065.

Alehosseini, A., Gomez-Mascaraque, L.G., Ghorani, B., Lopez-Rubio, A., 2019. Stabilization of a saffron extract through its encapsulation within electrospun/electrosprayed zein structures. Lebensm. Wiss. Technol. 113, 108280. https://doi.org/10.1016/j.lwt.2019.108280.

Amariei, N., Manea, L.R., Bertea, A.P., Bertea, A., Popa, A., 2017. The influence of polymer solution on the properties of electrospun 3D nanostructures. Int. Conf. Innov. Res. - Icir Euroinvent 209, 012092. https://doi.org/10.1088/1757-899x/209/1/012092.

Angel, N., Guo, L., Yan, F., Wang, H., Kong, L., 2020. Effect of processing parameters on the electrospinning of cellulose acetate studied by response surface methodology. J. Agric. Food Res. 2, 100015. https://doi.org/10.1016/j.jafr.2019.100015.

Bakowska, A., Kucharska, A.Z., Oszmianski, J., 2003. The effects of heating, UV irradiation, and storage on stability of the anthocyanin-polyphenol copigment complex. Food Chem. 81, 349–355. https://doi.org/10.1016/S0308-8146(02)00429-6.

Bao, Y., Cui, H., Tian, J., Ding, Y., Tian, Q., Zhang, W., Wang, M., Zang, Z., Sun, X., Li, D., Si, X., Li, B., 2021. Novel pH sensitivity and colorimetry-enhanced anthocyanin indicator films by chondroitin sulfate co-pigmentation for shrimp freshness monitoring. Food Control 131, 108441. https://doi.org/10.1016/j.foodcont.2021.108441.

Basdeki, A.M., Fatouros, D.G., Biliaderis, C.G., Moschakis, T., 2021. Physicochemical properties of human breast milk during the second year of lactation. Curr. Res. Food Sci. 4, 565–576. https://doi.org/10.1016/j.crfs.2021.08.001.

Bigi, A., Panzavolta, S., Rubini, K., 2004. Relationship between triple-helix content and mechanical properties of gelatin films. Biomaterials 25, 5675–5680. https://doi.org/10.1016/j.biomaterials.2004.01.033.

Buchweitz, M., Brauch, J., Carle, R., Kammerer, D.R., 2013a. Application of ferric anthocyanin chelates as natural blue food colorants in polysaccharide and gelatin based gels. Food Res. Int. 51, 274–282. https://doi.org/10.1016/j.foodres.2012.11.030.

Buchweitz, M., Brauch, J., Carle, R., Kammerer, D.R., 2013b. Colour and stability assessment of blue ferric anthocyanin chelates in liquid pectin-stabilised model systems. Food Chem. 138, 2026–2035. https://doi.org/10.1016/j.foodchem.2012.10.090.

Buzby, J.C., Farah-Wells, H., Hyman, J., 2014. The Estimated Amount, Value, and Calories of Postharvest Food Losses at the Retail and Consumer Levels in the United States. Economic Information Bulletin. https://doi.org/10.2139/ssrn.2501659.

Chen, H., Zhang, M., Bhandari, B., Yang, C., 2020. Novel pH-sensitive films containing curcumin and anthocyanins to monitor fish freshness. Food Hydrocolloids 100, 105438. https://doi.org/10.1016/j.foodhyd.2019.105438.

Chen, S.L., Wu, M., Lu, P., Gao, L., Yan, S., Wang, S.F., 2020. Development of pH indicator and antimicrobial cellulose nanofibre packaging film based on purple sweet potato anthocyanin and oregano essential oil. Int. J. Biol. Macromol. 149, 271–280. https://doi.org/10.1016/j.ijbiomac.2020.01.231.

Choi, I., Lee, J.Y., Lacroix, M., Han, J., 2017. Intelligent pH indicator film composed of agar/potato starch and anthocyanin extracts from purple sweet potato. Food Chem. 218, 122–128. https://doi.org/10.1016/j.foodchem.2016.09.050.

Clifford, M.N., 2000. Anthocyanins - nature, occurrence and dietary burden. J. Sci. Food Agric. 80, 1118–1125. https://doi.org/10.1002/(SICI)1097-0010(20000515)80:73.0.CO, 2-9.

Deng, L., Zhang, X., Li, Y., Que, F., Kang, X., Liu, Y., Feng, F., Zhang, H., 2018. Characterization of gelatin/zein nanofibers by hybrid electrospinning. Food Hydrocolloids 75, 72–80. https://doi.org/10.1016/j.foodhyd.2017.09.011.

Devarayan, K., Kim, B.S., 2015. Reversible and universal pH sensing cellulose nanofibers for health monitor. Sens. Actuators, B 209, 281–286. https://doi.org/10.1016/j.snb.2014.11.120.

El-Naggar, M.E., El-Newehy, M.H., Aldalbahi, A., Salem, W.M., Khattab, T.A., 2021. Immobilization of anthocyanin extract from red-cabbage into electrospun polyvinyl alcohol nanofibers for colorimetric selective detection of ferric ions. J. Environ. Chem. Eng. 9, 105072. https://doi.org/10.1016/j.jece.2021.105072.

Etxabide, A., Mate, J.I., Kilmartin, P.A., 2021. Effect of curcumin, betanin and anthocyanin containing colourants addition on gelatin films properties for intelligent films development. Food Hydrocolloids 115, 106593. https://doi.org/10.1016/j.foodhyd.2021.106593.

Ezati, P., Rhim, J.W., 2020. pH-responsive pectin-based multifunctional films incorporated with curcumin and sulfur nanoparticles. Carbohydr. Polym. 230, 115638. https://doi.org/10.1016/j.carbpol.2019.115638.

Ge, Y.J., Li, Y., Bai, Y., Yuan, C.H., Wu, C.H., Hu, Y.Q., 2020. Intelligent gelatin/oxidized chitin nanocrystals nanocomposite films containing black rice bran anthocyanins for fish freshness monitorings. Int. J. Biol. Macromol. 155, 1296–1306. https://doi.org/10.1016/j.ijbiomac.2019.11.101.

Goodarzi, M.M., Moradi, M., Tajik, H., Forough, M., Ezati, P., Kuswandi, B., 2020. Development of an easy-to-use colorimetric pH label with starch and carrot anthocyanins for milk shelf life assessment. Int. J. Biol. Macromol. 153, 240–247. https://doi.org/10.1016/j.ijbiomac.2020.03.014.

Gustavsson, J., Cederberg, C., Sonesson, U., Otterdijk, R., Mcybeck, A., 2011. Global Food Losses and Food Waste: Extent, Causes and Prevention, vol. 38. Food and Agriculture Organization of the United Nations.

He, Z., Xu, M., Zeng, M., Qin, F., Chen, J., 2016. Preheated milk proteins improve the stability of grape skin anthocyanins extracts. Food Chem. 210, 221–227. https://doi.org/10.1016/j.foodchem.2016.04.116.

Jia, R.N., Tian, W.G., Bai, H.T., Zhang, J.M., Wang, S., Zhang, J., 2019. Amine-responsive cellulose-based ratiometric fluorescent materials for real-time and visual detection of shrimp and crab freshness. Nat. Commun. 10 https://doi.org/10.1038/s41467-019-08675-3.

Jiang, G., Hou, X., Zeng, X., Zhang, C., Wu, H., Shen, G., Li, S., Luo, Q., Li, M., Liu, X., Chen, A., Wang, Z., Zhang, Z., 2020. Preparation and characterization of indicator films from carboxymethyl-cellulose/starch and purple sweet potato (Ipomoea batatas (L.) lam) anthocyanins for monitoring fish freshness. Int. J. Biol. Macromol. 143, 359–372. https://doi.org/10.1016/j.ijbiomac.2019.12.024.

Khaodee, W., Aeungmaitrepirom, W., Tuntulani, T., 2014. Effectively simultaneous naked-eye detection of Cu(II), Pb(II), Al(III) and Fe(III) using cyanidin extracted from red cabbage as chelating agent. Spectrochim. Acta, Part A 126, 98–104. https://doi.org/10.1016/j.saa.2014.01.125.

Kumar, T.S.M., Kumar, K.S., Rajini, N., Siengchin, S., Ayrilmis, N., Rajulu, A.V., 2019. A comprehensive review of electrospun nanofibers: food and packaging perspective. Composites Part B 175, 107074. https://doi.org/10.1016/j.compositesb.2019.107074.

Lee, D.S., Kim, Y., Song, Y., Lee, J.H., Lee, S., Yoo, S.H., 2016. Development of a gluten-free rice noodle by utilizing protein-polyphenol interaction between soy protein isolate and extract of Acanthopanax sessiliflorus. J. Sci. Food Agric. 96, 1037–1043. https://doi.org/10.1002/jsfa.7193.

Li, Y.N., Wu, K.X., Wang, B.H., Li, X.Z., 2021. Colorimetric indicator based on purple tomato anthocyanins and chitosan for application in intelligent packaging. Int. J. Biol. Macromol. 174, 370–376. https://doi.org/10.1016/j.ijbiomac.2021.01.182.

Liu, J., Wang, H., Guo, M., Li, L., Chen, M., Jiang, S., Li, X., Jiang, S., 2019. Extract from Lycium ruthenicum Murr. Incorporating κ-carrageenan colorimetric film with a wide pH–sensing range for food freshness monitoring. Food Hydrocolloids 94, 1–10. https://doi.org/10.1016/j.foodhyd.2019.03.008.

Loudiyi, M., Temiz, H.T., Sahar, A., Ahmad, M.H., At-Kaddour, A., 2020. Spectroscopic techniques for monitoring changes in the quality of milk and other dairy products during processing and storage. Crit. Rev. Food Sci. Nutr. 1–25 https://doi.org/10.1080/10408398.2020.1862754.

Lu, M., Shiau, Y., Wong, J., Lin, R., Kravis, H., Blackmon, T., Pakzad, T., Jen, T., Cheng, A., Chang, J., 2013. Milk spoilage: methods and practices of detecting milk quality, 04 Food Nutr. Sci. 113–123. https://doi.org/10.4236/fns.2013.47A014.

Ma, Q.Y., Ren, Y.M., Gu, Z.X., Wang, L.J., 2017. Developing an intelligent film containing Vitis amurensis husk extracts: the effects of pH value of the film-forming solution. J. Clean. Prod. 166, 851–859. https://doi.org/10.1016/j.jclepro.2017.08.099.

Ma, Y.L., Li, S.Y., Ji, T.T., Wu, W.Q., Sameen, D.E., Ahmed, S., Qin, W., Dai, J.W., Liu, Y. W., 2020. Development and optimization of dynamic gelatin/chitosan nanoparticles incorporated with blueberry anthocyanins for milk freshness monitoring. Carbohydr. Polym. 247, 116738. https://doi.org/10.1016/j.carbpol.2020.116738.

Madeira, P.P., Loureiro, J.A., Freire, M.G., Coutinho, J.A.P., 2019. Solvatochromism as a new tool to distinguish structurally similar compounds. J. Mol. Liq. 274, 740–745. https://doi.org/10.1016/j.molliq.2018.11.050.

Mohd, P., Khan, A., Farooqui, M., 2011. Analytical applications of plant extract as natural pH indicator: a review. J. Adv. Sci. Res. 2, 20–27. https://api.semanticscholar.org/CorpusID:99777556.

Montagna, E., Marzon, G.A., Torres, B.B., 2014. Development and Assessment of a Paper Electrophoresis Simulation Software for Chemical Equilibrium Teaching and Learning, vol. 12. Revista De Ensino De Bioquímica, p. 90. https://doi.org/10.16923/reb.v12i1.355.

Moradi, M., Tajik, H., Almasi, H., Forough, M., Ezati, P., 2019. A novel pH-sensing indicator based on bacterial cellulose nanofibers and black carrot anthocyanins for monitoring fish freshness. Carbohydr. Polym. 222, 115030. https://doi.org/10.1016/j.carbpol.2019.115030.

Pateiro, M., Domínguez, R., Bermúdez, R., Munekata, P.E.S., Zhang, W., Gagaoua, M., Lorenzo, J.M., 2019. Antioxidant active packaging systems to extend the shelf life of sliced cooked ham. Curr. Res. Food Sci. 1, 24–30. https://doi.org/10.1016/j.crfs.2019.10.002.

Prietto, L., Pinto, V.Z., Halal, S.E., Morais, M.D., Costa, J., Lim, L.T., Dias, A., Zavareze, E. R., 2017. Ultrafine fibers of zein and anthocyanins as natural pH indicator. J. Sci. Food Agric. 98, 2735–2741. https://doi.org/10.1002/jsfa.8769.

Priyadarshi, R., Ezati, P., Rhim, J.W., 2021. Recent advances in intelligent food packaging applications using natural food colorants. ACS Food Sci. Technol. 1, 124–138. https://doi.org/10.1021/acsfoodscitech.0c00039.

Renata, D.O.G., Bretas, R.E.S., Oréfice, R.L., 2016. Control of the hydrophilic/hydrophobic behavior of biodegradable natural polymers by decorating surfaces with nano- and micro-components. Adv. Polym. Technol. 37, 654–661. https://doi.org/10.1002/adv.21706.

Sanuja, S., Agalya, A., Umapathy, M.J., 2015. Synthesis and characterization of zinc oxide–neem oil–chitosan bionanocomposite for food packaging application. Int. J. Biol. Macromol. 74, 76–84. https://doi.org/10.1016/j.ijbiomac.2014.11.036.

Shaikh, S., Yaqoob, M., Aggarwal, P., 2021. An overview of biodegradable packaging in food industry. Curr. Res. Food Sci. 4, 503–520. https://doi.org/10.1016/j.crfs.2021.07.005.

Shi, C., Zhang, J., Jia, Z., Yang, X., Zhou, Z., 2020. Intelligent pH indicator films containing anthocyanins extracted from blueberry peel for monitoring tilapia fillet freshness. J. Sci. Food Agric. 101, 1800–1811. https://doi.org/10.1002/jsfa.10794.

Singh, S., Nwabor, O.F., Syukri, D.M., Voravuthikunchai, S.P., 2021. Biodegradable chitosan-poly(vinyl alcohol) intelligent films fortified with anthocyanins isolated from Clitoria ternatea and Carissa carandas for monitoring freshness of beverages. Int. J. Biol. Macromol. 182, 1015–1025. https://doi.org/10.1016/j.ijbiomac.2021.04.027.

Sun, W., Liu, Y., Jia, L., Saldaa, M., Dong, T., Jin, Y., Sun, W., 2020. A smart nanofibre sensor based on anthocyanin/poly-l-lactic acid for mutton freshness monitoring. Int. J. Food Sci. Technol. 56, 342–351. https://doi.org/10.1111/ijfs.14648.

Tan, C.C., Karim, A.A., Uthumporn, U., Ghazali, F.C., 2019. Effect of extraction temperature on the physicochemical properties of gelatine from the skin of black Tilapia (Oreochromis mossambicus). J. Phys. Sci. 30, 1–21. https://doi.org/10.21315/jps2019.30.s1.1.

Torrini, F., Renai, L., Scarano, S., Bubba, M.D., Palladino, P., Minunni, M., 2022. Colorimetric selective quantification of anthocyanins with catechol/pyrogallol moiety in edible plants upon zinc complexation. Talanta 240, 123156. https://doi.org/10.1016/j.talanta.2021.123156.

Ulrich, S., Moura, S.O., Diaz, Y., Clerc, M., Guex, A.G., de Alaniz, J.R., Martins, A., Neves, N.M., Rottmar, M., Rossi, R.M., Fortunato, G., Boesel, L.F., 2020. Electrospun colourimetric sensors for detecting volatile amines. Sens. Actuators, B 322, 128570. https://doi.org/10.1016/j.snb.2020.128570.

Wang, Y., Ding, W., Kou, L., Li, L., Wang, C., Wayne, I.I., 2015. A Non-destructive method to assess freshness of raw bovine milk using FT-NIR spectroscopy. J. Food Sci. Technol. 52, 5305–5310. https://doi.org/10.1007/s13197-014-1574-5.

Weston, M., Phan, M.A.T., Arcot, J., Chandrawati, R., 2020. Anthocyanin-based sensors derived from food waste as an active use-by date indicator for milk. Food Chem. 326, 127017. https://doi.org/10.1016/j.foodchem.2020.127017.

Wu, L.T., Tsai, I.L., Ho, Y.C., Hang, Y.H., Lin, C., Tsai, M.L., Mi, F.L., 2020. Active and intelligent gellan gum-based packaging films for controlling anthocyanins release and monitoring food freshness. Carbohydr. Polym. 254, 117410. https://doi.org/10.1016/j.carbpol.2020.117410.

Xie, Y.L., Zhu, X.L., Li, Y., Wang, C., 2018. Analysis of the pH-dependent Fe(III) ion chelating activity of anthocyanin extracted from black soybean [Glycine max (L.) merr.] coats. J. Agric. Food Chem. 66, 1131–1139. https://doi.org/10.1021/acs.jafc.7b04719.

Xue, C., Dong, S., 2014. Spectroscopic analysis of interaction between four kinds of flavonoids and bovine serum albumin. Chem. Res. 25, 152–157. https://doi.org/10.14002/j.hxya.2014.02.007.

Yang, Y.N., Lu, K.Y., Wang, P., Tsai, M.L., Mi, F.L., 2020. Development of bacterial cellulose/chitin multi-nanobers based smart films containing natural active microspheres and nanoparticles formed in situ. Carbohydr. Polym. 228, 115370. https://doi.org/10.1016/j.carbpol.2019.115370.

Yang, T.T., Yang, H.R., Fan, Y., Li, B.F., Hou, H., 2018. Interactions of quercetin, curcumin, epigallocatechin gallate and folic acid with gelatin. Int. J. Biol. Macromol. 118, 124–131. https://doi.org/10.1016/j.ijbiomac.2018.06.058.

Yi, K., Cheng, G., Xing, F., 2010. Gelatin/tannin complex nanospheres via molecular assembly. J. Appl. Polym. Sci. 101, 3125–3130. https://doi.org/10.1002/app.22416.

Zeng, P., Chen, X., Qin, Y.R., Zhang, Y.H., Wang, X.P., Wang, J.Y., Ning, Z.X., Ruan, Q.J., Zhang, Y.S., 2019. Preparation and characterization of a novel colorimetric indicator film based on gelatin/polyvinyl alcohol incorporating mulberry anthocyanin extracts tor whim for monitoring fish freshness. Food Res. Int. 126, 108604. https://doi.org/10.1016/j.foodres.2019.108604.

Zhang, H.J., Hou, A.Q., Xie, K.L., Gao, A.Q., 2019. Smart color-changing paper packaging sensors with pH sensitive chromophores based on azo-anthraquinone reactive dyes. Sens. Actuators, B 286, 362–369. https://doi.org/10.1016/j.snb.2019.01.165.

Zhang, K., Huang, T.S., Yan, H., Hu, X., Ren, T., 2019. Novel pH-sensitive films based on starch/polyvinyl alcohol and food anthocyanins as a visual indicator of shrimp deterioration. Int. J. Biol. Macromol. 145, 768–776. https://doi.org/10.1016/j.ijbiomac.2019.12.159.

Zhang, Y., Lu, Y., Yang, Y., Li, S., Wang, C., Wang, C., Zhang, T., 2021. Comparison of non-covalent binding interactions between three whey proteins and chlorogenic acid: spectroscopic analysis and molecular docking. Food Biosci. 41, 101035. https://doi.org/10.1016/j.fbio.2021.101035.

Zhao, J., Pan, F., Li, P., Zhao, C., Jiang, Z., Zhang, P., Cao, X., 2013. Fabrication of ultrathin membrane via layer-by-layer self-assembly driven by hydrophobic interaction towards high separation performance. ACS Appl. Mater. Interfaces 5, 13275–13283. https://doi.org/10.1021/am404268z.